ChemComm

Accepted Manuscript

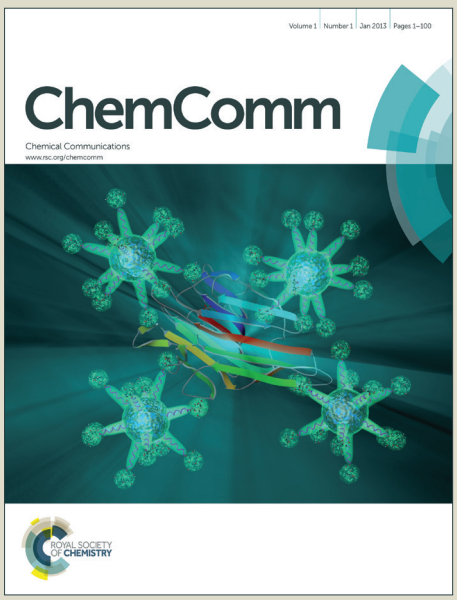

ROYAL SOCIETY OF CHEMISTRY

www.rsc.org/chemcomm

Journal Name

RSCPublishing

COMMUNICATION

Synthesized Ultrathin MoS_2 Nanosheets Perpendicular to Graphene for Catalysis of Hydrogen Evolution Reaction

Z. H. Deng, L. Li, W. Ding, K. Xiong and Z. D. Wei*

Cite this: DOI: 10.1039/xoxxoooooox

Received ooth January 2012,
Accepted ooth January 2012

DOI: 10.1039/xoxxoooooox

www.rsc.org/

We synthesize the ultrathin MoS_2 nanosheets perpendicular to reduced graphene oxides($MoS_2 \perp$ RGO) as an electrocatalyst, which exhibits excellent catalytic activity and good stability for the hydrogen evolution reaction(HER) in acidic medium.

The layered molybdenum disulfide (MoS_2) has attracted a lot of attention as a promising electrocatalyst and photocatalyst for the hydrogen evolution reaction (HER) from water.[1] Although Pt-group metals are the most effective HER catalysts, their applications are severely limited by the high cost and the low abundance of Pt. A great deal of evidence has shown that MoS_2 is a suitable candidate for the HER in acidic medium.

As an efficient HER catalyst, two major challenges should be solved: exfoliating stacked MoS_2 layers to increase the density of the active sites and improving the electrical contacts to active sites.[1] Theoretical calculations and experimental studies have revealed that the HER active sites are located at the edges rather than on the basal surfaces of a MoS_2 sheet.[2-8] Therefore, the ultrathin MoS_2 nanosheets have been used to increase the density of the active edges of the catalyst.[9] However, the edges of the ultrathin MoS_2 are undercoordinated and thermo-dynamically unstable, which is easy to curl up into inorganic fullerene structures.[10] Additionally, the low conductivity of MoS_2 catalyst limits electron transport in the catalyst and leads to poor catalytic performance. MoS_2 can exist in various polymorphs, in which 2H-MoS_2 is the semi-conducting and thermodynamically stable phase with edge-sharing MoS_6 trigonal prisms, while 1T-MoS_2 is the metallic and metastable phase with edge-sharing MoS_6 octahedra. The 1T-MoS_2 nanosheets, obtained via lithium intercalation exfoliation of 2H-MoS_2 nanosheets, show high electron transport rate and high HER activity.[11] But a higher temperature over 95°C will cause 1T-MoS_2 quickly convert to the 2H phase.[12]

Recently, the edges of nanostructure 2H-MoS_2 have been observed to be more conductive,[13] suggesting that electron may be passed along the edge from the support substrate to the active edges. Such observation implies that MoS_2 nanosheets perpendicular to the conductive surface would be advantageous to design an efficient HER catalyst.[1] Herein, we synthesized the ultrathin MoS_2 nanosheets perpendicular to reduced graphene oxides ($MoS_2 \perp$RGO) by a hydrothermal method as an efficient HER catalyst. The MoS_2 nanoparticles lay flat on the graphene by a solvothermal reduction was previously reported.[14] However, it is not reported that synthesized ultrathin MoS_2 nanosheets perpendicular to the support substrate with enhanced electrical transport and high active-sites density. Graphene, single-layer sheets of sp^2-hybridized carbon atoms, is an effective support substrate for growing and anchoring of MoS_2.[15] In our work, we have shown that the oxygen functional groups of graphene play an anchoring role in fixing MoS_2 nanosheets perpendicular to graphene. The characterization results show that ultrathin MoS_2 nanosheets are uniformly and perpendicularly grown on RGO. As expected, electrochemical evaluations show that the $MoS_2 \perp$RGO catalyst exhibits excellent electronic conductivity, high density of active edges, high HER electrocatalytic activity and good stability in acidic electrolytes.

Fig.1 (top) shows the synthesis schematic of the $MoS_2 \perp$RGO catalyst. The ultrathin MoS_2 nanosheets perpendicular to RGO were synthesized *via* a hydrothermal synthesis using the H_2NCSNH_2 and $(NH_4)_6Mo_7O_{24}\cdot 4H_2O$ in a highly oxidized graphene aqueous solution at 180℃ for 30 h. The molar ratio of Mo to S in the precursors was kept in 1:8. The excess of thiourea was employed as a reducing agent and an efficient additive to make MoS_2 perpendicular to RGO.[16] We could speculate the growth mechanism of $MoS_2 \perp$RGO as below:

during the hydrothermal synthesis, the S atoms bond to active sites of RGO and form C=S/C-S bonds; then these S atoms act as crystal seeds for the nucleation of MoS_2. When the highly oxidized graphene is used as support, a high density nucleation of MoS_2 is obtained. Thus, the MoS_2 nanosheets grow perpendicularly on RGO due to the space limitations.

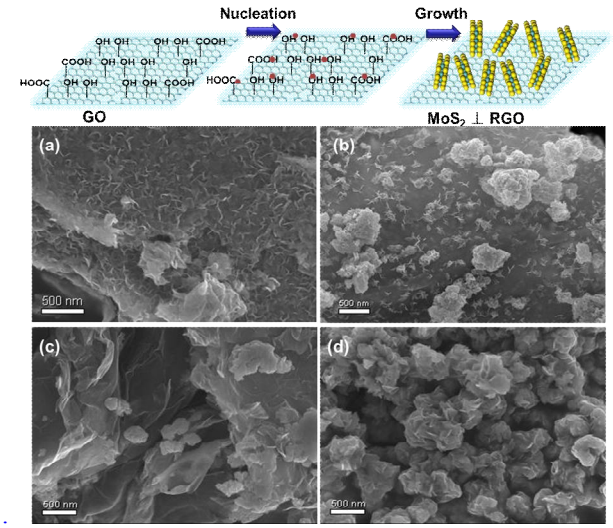

Fig. 1 Schematic representation of the synthesis of the $MoS_2 \perp$ RGO catalyst (top); FESEM images of as-synthesized MoS_2 loaded on the highly oxidized graphene ($MoS_2 \perp$ RGO) (a); and the mildly oxidized graphene (MoS_2/RGO) (b); a direct mixture of MoS_2 and graphene sheets (MoS_2/G) (c), MoS_2 obtained without graphene (MoS_2) (d).

Fig. S1 (see in ESI) shows more than 57.7% of the C species in the highly oxidized graphene were oxidized (C=O 31.02%, COOH 26.74%), whereas the oxidized C species in mildly oxidized graphene only account for 33.9% (C=O 20.54%, COOH 13.36%). Field emission scanning electron microscopy (FESEM) images (Fig. 1) clearly showed that the morphology of as-synthesized samples. With participation of the highly oxidized graphene into the hydrothermal synthesis solution, the ultrathin MoS_2 nanosheets with an average wide of ~100 nm were uniformly formed on RGO as shown in Fig. 1a and Fig. 2c. Each individual MoS_2 nanosheet is perpendicular to the wrinkle graphene substrate with abundantly exposed edges. With participation of the mildly oxidized graphene, only few of MoS_2 nanosheet was formed on RGO as shown in Fig 1b, while most of them agglomerate together. The simple mixture of graphene and MoS_2 only led to poor dispersion as shown in Fig.1c. The serious agglomeration and stacked of MoS_2 was observed when no supports were used, as shown in Fig. 1d. These results indicate that the oxidation degree of graphene plays an important role in determining the final morphology of MoS_2 nanosheets, and it will result in different exposed active edge sites of the MoS_2 nanosheets.

Transmission electron microscopy (TEM) images (Fig.2a) show that the MoS_2 nanosheets are uniformly and perpendicularly grown on RGO. While the support-free MoS_2 exhibited serious agglomeration (Fig. 2d). The high-resolution transmission electron microscopy (HRTEM) images further demonstrate the morphology of $MoS_2 \perp$ RGO catalyst. Fig. 2b show the lattice fringes with a distance of 0.61 nm matching well with *d* spacing of (002) planes of 2H-MoS_2, but no lattice fringes in the outer part corresponding to the wrinkle graphene substrate. In addition, the statistical layer number from 124 different sheets of MoS_2 was shown in the inset of Fig.2a. Most of nanosheets (~84%) with average thickness around 3.5nm are comprised with about ~6 layers of the monatomic sheet. The measured thickness was consistent with those previously reported value for exfoliated MoS_2.[17, 18] These results indicate the ultrathin nature of as-synthesized MoS_2 nanosheets. The element distribution of the $MoS_2 \perp$ RGO catalyst were examined using a scan transmission electron microscope (STEM) equipped with a typical electron energy loss spectrum (EELS), which the electron beam was focused on 300nm line and scanned to form compositional maps. The uniform distribution of Mo and S with a Mo: S (at%) ratio of 1:2.31 (Fig. S2) indicates that there are abundant unsaturated ligands S-dangling on the edges of the $MoS_2 \perp$ RGO catalyst.

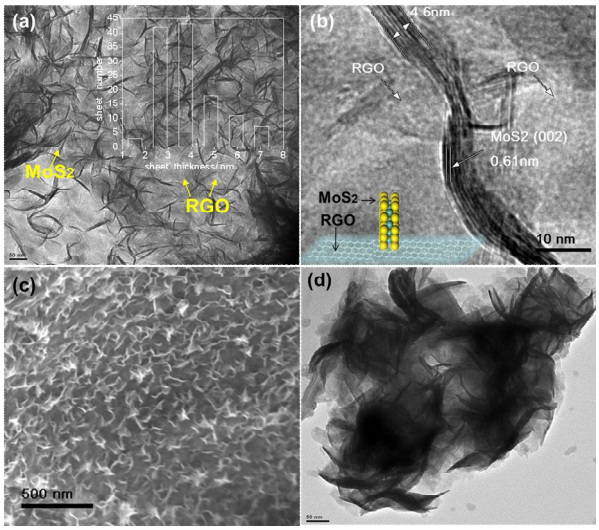

Fig. 2 (a) TEM of the $MoS_2 \perp$ RGO catalyst and statistical observations from 124 different nanosheets of the $MoS_2 \perp$ RGO catalyst (inset); (b) HRTEM of the $MoS_2 \perp$ RGO catalyst; (c) FESEM of the $MoS_2 \perp$ RGO catalyst; and (d) TEM of the support-free MoS_2.

An extensive physical characterization was conducted to further reveal the morphology of the $MoS_2 \perp$ RGO catalyst. Fig.S3 shows the XRD patterns of the samples. The diffraction peaks at 2θ=14.38, 32.68 and 58.33° correspond to the (002), (100) and (110) planes of 2H-MoS_2, respectively. The diffraction peaks in the $MoS_2 \perp$ RGO catalyst (Fig. S3c) are weaker and broader than those of support-free MoS_2 (Fig. S3b). It suggests that presence of the highly oxidized graphene results in more ultrathin MoS_2 nanosheets production and lower crystalline structure. X-ray photoelectron spectroscopy (XPS) shows that the $MoS_2 \perp$ RGO catalyst consists of Mo, S, C and O element (Fig. S4a). The C1s XPS spectra in $MoS_2 \perp$ RGO (Fig. S4b) shows a dominated C-C peak with a small peak related to oxygen-containing group, confirming the effective reduction of GO to

RGO during the hydrothermal process.[19a] The S2p XPS spectra of the $MoS_2 \perp$RGO (Fig. S4c) exhibits the peaks of $S2p_{3/2}$ and $S2p_{1/2}$ at 162.27 and 163.30eV, respectively. These values are slightly higher than that of S2p in the support-free MoS_2. The Mo3d spectra of $MoS_2 \perp$RGO shows 0.2 eV higher binding energies of $Mo3d_{5/2}$ and $Mo3d_{3/2}$ (229.46 and 232.60 eV) than that of the support-free MoS_2 (229.26 and 232.40 eV) as shown in Fig. S4d. The high resolution XPS of O1s has be shown in Fig.S5. The O1s XPS spectrum in the $MoS_2 \perp$RGO catalyst is weaker than those of in GO, indicating that GO effectively reduced to RGO. The O1s binding energy shifts toward the low energy due to the difference between the RGO and the GO rather than the formation of Mo-O bonds because there is no evidence that support Mo-O bond presence (530eV).[19b, 20a] The high resolution XPS of S2p shows three peaks (Fig. S5). The weak peaks at 163.8 eV is assigned to the C-S bond, [19c] indicating that the C-S bond is formed. In addition, Fourier transform infrared spectroscopy (FTIR) spectra (Fig.S6) reveals that GO displays three peaks at 3423, 1631-1410 and 1010 cm^{-1} characteristic of oxygen-containing group, i.e., hydroxyl, carboxyl and epoxy groups,[20b] respectively. The $MoS_2 \perp$RGO exhibits new FTIR peaks at 1205 and 1140 cm^{-1}, indicating the C=S asymmetric and symmetric stretching modes.[20c] The additional peak at 757 cm^{-1} is assigned to C-S stretching vibration.[20d] In a word, the interaction between the C and S, most likely unsaturated S on the edges of the MoS_2 rather than the saturated S in the planes of the MoS_2, induces MoS_2 nanosheets perpendicularly grow on RGO.

The HER catalytic activity of the $MoS_2 \perp$RGO catalyst was evaluated by using rotating disc electrode (RDE) in a typical three-electrode cell in N_2-saturated 0.5M H_2SO_4 solution. As a contrast, the HER catalytic performance of the support-free MoS_2, MoS_2 mix RGO, MoS_2/RGO and Pt/C (20 wt% Pt on Vulcan carbon black) were also measured. As shown in Fig. 3a, the $MoS_2 \perp$RGO catalyst exhibited an excellent activity for the HER. The overpotential is as small as 172 mV *vs.* RHE at HER current of 10 $mA \cdot cm^{-2}$ (η_{10}), while the support-free MoS_2, MoS_2/G and MoS_2/RGO exhibited little HRE activity with high η_{10} of 402, 288, 252mV, respectively. To obtain further insight into the HER on the various catalysts, the Tafel slopes were investigated. The linear portions of the Tafel plots (Fig. 3c) were fit to the Tafel equation, yielding Tafel slopes of 30, 43, 94 $mV \cdot dec^{-1}$ for Pt/C, $MoS_2 \perp$RGO and the support-free MoS_2, respectively. The results are agreement with earlier reports,[14] suggesting that electrochemical desorption is the rate-limiting step in the HER catalyzed by the $MoS_2 \perp$RGO catalyst. A summary of the η_{10}, Tafel slopes and loading of the reported various MoS_2 HER catalysts is shown in Table S1. The $MoS_2 \perp$RGO shows a relatively lower Tafel slope and η_{10}. It can be inferred that there are more exposed edges in $MoS_2 \perp$RGO, providing more active sites, which can generate a larger current at low overpotential.

To investigate the effect of graphene content on the $MoS_2 \perp$RGO catalyst, the weight ratios of GO to $MoS_2 \perp$RGO were varied from 0 to 10, 15 and 20wt% by varying the weight of oxidized graphene. The resulting samples were labeled as $MoS_2 \perp$RGO(x), where x=0, 10, 15 and 20%, respectively. Unless otherwise stated, $MoS_2 \perp$RGO refers to the $MoS_2 \perp$RGO(15%). Fig.3b shows electrochemical tests on a series of $MoS_2 \perp$RGO(x) catalysts. The content of graphene plays a significant influence on the HER activity. The $MoS_2 \perp$RGO(15%) obtained the highest HER activity. The XRD patterns in Fig. S7 illustrated the lowest crystallinity in $MoS_2 \perp$RGO(15%). These data indicate that abundant unsaturated edge in MoS_2 nanosheets may be the HER active sites.

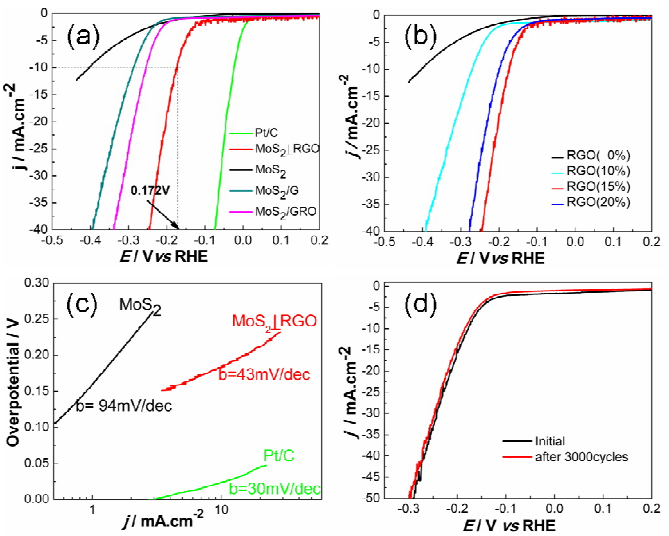

Fig. 3 (a) Polarization curves of several catalysts and (b) Polarization curves of $MoS_2 \perp$RGO (x) in 0.5M H_2SO_4 at rate scan 5mV/s; (c) Tafel plots of several catalysts; (d) Stability test for the $MoS_2 \perp$RGO catalyst.

We speculate that the perpendicular morphology of the ultrathin MoS_2 nanaosheets was the major reason for the HER activity enhancement. The excellent catalytic activity of the $MoS_2 \perp$RGO catalyst may arise from the synergetic effect of good electron transport and abundant active edge sites. Electrochemical impedance spectroscopy (EIS) performed at high frequency revealed the electrical resistance of the catalysts. As shown in Fig. S8, the electrical resistance of the $MoS_2 \perp$RGO(15%) catalysts reaches the lowest point among the $MoS_2 \perp$RGO(x) catalysts. The electrical resistance of $MoS_2 \perp$RGO(15%), $MoS_2 \perp$RGO(20%) and MoS_2 is determined to be 5, 10, and 435Ω, respectively. The $MoS_2 \perp$RGO (15%) catalyst is around 87 times more conductive than the support-free MoS_2 catalyst. The results clearly show that the conductivity of the $MoS_2 \perp$RGO(x) catalysts is agreement with the HER catalytic activity.

The capacitance of the double layer (C_{dl}) is used to estimate the effective surface area of the solid-liquid interface. The C_{dl} is determined using a cyclic-voltammetry (CV) method, which is expected to be linearly proportional to effective active site. The current response in region of 0.1~0.2 V *vs.* RHE is attributed to the charging of the double layer (Fig. S9). Fig. S10 shows the $MoS_2 \perp$RGO(x) catalysts have a much larger C_{dl} than the support-free MoS_2 catalyst. The Brunauer-Emmet-

Teller (BET) specific surface areas showed no significant different between the $MoS_2 \perp$ RGO (54.7 $m^2 \cdot g^{-1}$) and the support-free MoS_2 (50.0 $m^2 \cdot g^{-1}$). These results indicate that the catalytic activity lies in the active edge sites rather than in the total surface areas. The largest effective edge sites among the different catalysts was observed for $MoS_2 \perp$RGO(15%) and decreased in the order of $MoS_2 \perp$RGO(15%) > $MoS_2 \perp$ RGO(20%) > $MoS_2 \perp$RGO(10%) > MoS_2 (Table S2). The active edge sites in $MoS_2 \perp$RGO(15%) catalyst is 13.6 times higher than that in the support-free MoS_2. The results suggeste that the HER catalytic activity deeply correlate with the effective active edge sites.

The stability of the $MoS_2 \perp$RGO catalyst was evaluated by cycling the electrode at 100 $mV \cdot s^{-1}$ from -0.4 to 0.6 V in N_2-saturated 0.5M H_2SO_4. The performance of the $MoS_2 \perp$RGO catalyst after 3000 cycles (Fig. 3d) showed negligible loss relative to the fresh electrode, indicating a good stability of the $MoS_2 \perp$RGO catalyst.

Conclusions

In conclusion, we have synthesized ultrathin MoS_2 nanosheets perpendicular to RGO by a facile hydrothermal method. The oxidation degree of graphene plays a key role in controlling morphology and electrochemical performance of the MoS_2 nanosheets. The perpendicular morphology MoS_2 on RGO improves electron transport along the individual MoS_2 nanosheets and increases the density of the active edges of the catalyst. The fast electron transport and ion diffusion in the catalyst is thus benefited, leading to a sufficient electrochemical active-site for the HER. Electrochemical evaluations revealed that the $MoS_2 \perp$ RGO catalyst demonstrated a high density of active edges, excellent electronic conductivity, high HER catalytic activity and good stability in acidic electrolytes. It is demonstrated that it is feasible to produce ultrathin MoS_2 nanosheets perpendicular to the graphene by the hydrothermal method. This method could be extended to design other layered materials for application ranging from catalysis, sensors, supercapacitors to lithium-ion batteries.

This work was financially supported by China National 973 Program (2012CB720300), by NSFC of China (Grant Nos. 21306232 and 51072239) and by the Fundamental Research Funds for the Central Universities (CQDXWL-2012-043).

Notes and references

The State Key Laboratory of Power Transmission Equipment & System Security and New Technology, College of Chemistry and Chemical Engineering, Chongqing University, Chongqing, 400044(China)
Fax: +86 23 65102531;
E-mail: zdwei@cqu.edu.cn (Wei)

†Electronic Supplementary Information(ESI) available: the details of experimental procedures, physical characterization and electrochemical measurements. See DOI: 10.1039/c000000x/

1 A. B. Laursen, S. Kegnaes, S. Dahl, I. Chorkendorff,*Energ Environ Sci.*2012, **5**, 5577.
2 H. S. S. Ramakrishna Matte, A. Gomathi, A. K. Manna, D. J. Late, R.Datta, S. K. Pati, C. N. R. Rao, *Angew. Chem. Int. Ed.* 2010, **49**, 4059.
3 Z. Chen, D. Cummins, B. N. Reinecke, E. Clark, M. K. Sunkara, T. F.Jaramillo, *Nano Lett.,* 2011, **11**, 4168.
4 (*a*) J. V. Lauritsen, J. Kibsgaard, S. Helveg, H. Topsoe, B. S. Clausen, E.Lagsgaard, F. Besenbacher, *Nat. Nanotechnol.* 2007, **2**, 53; (*b*) P. Ge, M. D. Scanlon, P. Peljo, X. Bian, H. Vubrel, A. O'Neill, J. N. Coleman, M. Cantoni, X. Hu, K. Kontturi, B. Liu, H. H. Girault, *Chem. Commun*. 2012, **48**, 6484; (*c*) E. G. S. Firmiano, M. A. L. Cordeiro, A. C. Rabelo, C. J. Dalmaschio, A. N. Pinheiro, E. C. Pereira, E. R. Leite, *Chem. Commun*. 2012, **48**, 7687.
5 J. D. Benck, Z. Chen, L. Y. Kuritzky, A. J. Forman, T. F. Jaramillo,*ACS Catal.* 2012, **2**, 1916.
6 (*a*) X. Zheng, J. Xu, K. Yan, H. Wang, Z. Wang, S. Yang,*Chem. Mater.*2014, **26**, 2344;(*b*) K. Bindumadhavan, S. K. Srivastava, S. Mahanty, *Chem. Commun*. 2013, **49,**1823.
7 Y. Yan, B.Y. Xia, X. Y. Qi, H. B. Wang, R. Xu, J. Y. Wang, H. Zhang, X. Wang, *Chem. Commun*. 2013.**49**, 4884.
8 Z. Y. Lu, H. C. Zhang, W. Zhu, X. Y. Yu, Y. Kuang, Z. Chang, X. D. Lei, X. M. Sun,*Chem. Commun*. 2013, **49**, 7516.
9 Y. Yan, B. Xia, X. Ge, Z. Liu, *ACS Appl. Mater. Interfaces*. 2013, **5**, 12794.
10 R. Tenne, M. Redlich, *Chem. Soc. Rev.* 2010, **39,** 1423.
11 M. A. Lukowski, A. S. Daniel, F. Meng, A. Forticaux, L. Li, S. Jin, *J. Am. Chem. Soc*. 2013, **135,** 10274.
12 F. Wypych, R. Schollhorn, *J. Chem. Soc., Chem. Commun*. 1992, **19**, 1386.
13 M. V. Bollinger, J. V. Lauritsen, K. W. Jacobsen, J. K. Nørskov, S. Helveg, F. Besenbacher, *Phys. Rev. Lett.* 2001, **87,** 196803.
14 Y. Li, H. Wang, L. Xie, Y. Liang, G. Hong, H. J. Dai, *J. Am. Chem. Soc.*2011, **133**, 7296.
15 C. Lee, H. Yan, L. E. Brus, T. F. Heinz, J. Hone, S. Ryu, *ACS Nano.* 2010, **4**, 2695.
16 Q. Xiang, J. Yu, M. Jaroniec, *J. Am. Chem. Soc*. 2012, **134**, 6575.
17 B. Radisavljevic, A. Radenovic, J. Brivio, V. Giacometti, A. Kis, *Nat. Nanotechnology*. 2011, **6**, 147.
18 H. L. Wang, J. T. Robinson, G. Diankov, H. J. Dai, *J. Am. Chem. Soc.* 2010, **132**, 3270.
19 (a) H. J. Shin, K. K. Kim, A. Benayad, S. M. Yoon, H. K. I.Park, S. Jung,; M. H. Jin, H. K. Jeong, J. M. Kim, et al, *Adv, Funct .Mater.*2009, **19**, 1987; (b) B. S. Okan, A. Yürüm, N. Gorgülü, S. A. Gürsel, Y. Yürüm. *Ind. Eng. Chem. Res.* 2011, **50**, 12562;(c) Z. Liu , H. Nie , Z. Yang , J. Zhang , Z. Jin , Y. Lu , Z. Xiao , S. Huang ,*Nanoscale,*2013, **5**, 3283.
20 (a) Y. M. Sun, X. L. Hu, W. Luo, Y. H. Huang, *ACS Nano*, 2011, **5**, 7100; (b) X. Yang, X. Wang, J. Yang, J. Li, L. Wan, *Chem. Phys. Lett.* 2013, **570**, 125; (c) P. Cao, J. Yao, B. Ren, R. Gu, Z. Tian. *J. Phys. Chem. B,* 2002, **106 (39)**, 1050; (d) S. Bloxham, O. E. Lorka, R. Jakubėnas, G. Niaura. *CHEMIJA*, 2002, **13**, 185.